

Consolidating a Link Centered Neural Connectivity Framework with Directed Transfer Function Asymptotics

Luiz A. Baccalá Daniel Y. Takahashi Koichi Sameshima

January 26, 2015

Abstract

We present a unified mathematical derivation of the asymptotic behaviour of three of the main forms of *directed transfer function* (DTF) complementing recent partial directed coherence (PDC) results [3]. Based on these results and numerical examples we argue for a new directed ‘link’ centered neural connectivity framework to replace the widespread correlation based effective/functional network concepts so that directed network influences between structures become classified as to whether links are *active* in a *direct* or in an *indirect* way thereby leading to the new notions of *Granger connectivity* and *Granger influenciability* which are more descriptive than speaking of Granger causality alone.

1 Introduction

Introduced as a frequency domain characterization of the interaction between multiple neural structures *directed transfer function* (DTF) [16] can be thought as a factor in the coherence between pairs of observed time series [5]. A historical perspective on DTF by their authors can be found in [17] together with its many variants.

On a par with it, stands *partial directed coherence* (PDC) [5] as its dual measure. The chief distinction between them is that PDC captures *active* immediate directional coupling between structures whereas DTF, in general, portrays the existence of directional signal propagation even if it is only indirect, by going through intermediate structures rather through immediate direct causal influence [6]. DTF, therefore, represents signal ‘*reachability*’ in a graph theoretical sense whereas PDC is akin to an adjacency matrix description [13].

Since DTF’s introduction, we examined two of its closely related variants (a) directed coherence (DC) [2] which is DTF’s scale invariant form (and dual to generalized PDC (*gPDC*)[8]) and (b) information DTF (*ιDTF*) which is an information theoretic generalization of DTF, dual to information PDC (*ιPDC*), both of which provide accurate size effect information [26, 27, 28].

In this paper, we derive and illustrate inference results for the above DTF variants from a unified perspective closely paralleling the inference results in [3] and further illustrated in [22] for PDC and its variants. The importance of accurate asymptotics for DTF is that jointly DTF and PDC allow extending the current paradigm of effective/function connectivity to a more general and informative context [7].

After briefly reviewing DTF's formulations (Sec. 2) together with a summary of the unified asymptotic results (Sec. 3), numerical illustrations (Sec. 4) discuss some implications of the results as further elaborated in Sec. 5 with their implications for the new connectivity analysis paradigm we proposed in [7]. For reader convenience, mathematical details are left to the Appendix whose implementation is to appear in the next release of the AsympPDC package [3].

2 Background

The departure point for defining all DTF related variants is an adequately fitted multivariate autoregressive time series (i.e. vector time series) model to which a multivariate signal $\mathbf{x}(n)$ made up by $x_k(n)$, $k = 1, \dots, K$ simultaneously acquired time series conforms to

$$\mathbf{x}(n) = \sum_{l=1}^p \mathbf{A}(l) \mathbf{x}(n-l) + \mathbf{w}(n), \quad (1)$$

where $\mathbf{w}(n)$ stands for a zero mean white innovations process of with $\Sigma_{\mathbf{w}} = [\sigma_{ij}]$ as its covariance matrix and p is the model order. The $a_{ij}(l)$ coefficients composing each $\mathbf{A}(l)$ matrix describe the lagged effect of the j -th on the i -th series, wherefrom one can also define a frequency domain representation of (1) via the $\bar{\mathbf{A}}(f)$ matrix whose entries are given by

$$\bar{A}_{ij}(\lambda) = \begin{cases} 1 - \sum_{l=1}^p a_{ij}(l) e^{-j2\pi\lambda l}, & \text{if } i = j \\ - \sum_{l=1}^p a_{ij}(l) e^{-j2\pi\lambda l}, & \text{otherwise} \end{cases} \quad (2)$$

where $\mathbf{j} = \sqrt{-1}$, so that one may define

$$\mathbf{H}(\lambda) = \bar{\mathbf{A}}^{-1}(\lambda) \quad (3)$$

with $H_{ij}(\lambda)$ entries and rows denoted \mathbf{h}_i . This leads to a general expression

$$\gamma_{ij}(\lambda) = \frac{s \bar{H}_{ij}(\lambda)}{\sqrt{\mathbf{h}_i^H(\lambda) \mathbf{S} \mathbf{h}_i(\lambda)}} \quad (4)$$

summarizing all the forms of DTF from j to i considered herein. The superscript H denotes the usual Hermitian transpose. The reader should be forewarned to use the adequate expression for s and \mathbf{S} to obtain each DTF variant in (4) using Table 1.

Table 1: Defining variables according to DTF type in (4)

variable	DTF	DC	ι DTF
s	1	$\sigma_{ii}^{1/2}$	$\sigma_{ii}^{1/2}$
\mathbf{S}	\mathbf{I}_K	$(\mathbf{I}_K \odot \Sigma_{\mathbf{w}})$	$\Sigma_{\mathbf{w}}$

3 Result Overview

The statistical behaviour of (4) in terms of the number of times series data points (n_s) can be approximated invoking the *delta* method [30] consisting of an appropriate Taylor expansion of the statistics, leading, under mild assumptions, to the following results:

3.1 Confidence Intervals

In most applications, because n_s is large, usually only the first Taylor derivative suffices. In the present context, parameter asymptotic normality implies that DTF's point estimate will also be asymptotically normal, i.e.

$$\sqrt{n_s}(|\hat{\gamma}_{ij}(\lambda)|^2 - |\gamma_{ij}(\lambda)|^2) \xrightarrow{d} \mathcal{N}(0, \gamma^2(\lambda)), \quad (5)$$

where $\gamma^2(\lambda)$ is a frequency dependent variance whose full disclosure requires the introduction of further notation and is postponed to the Appendix.

3.2 Null Hypothesis Test

Under the null hypothesis,

$$H_0 : |\gamma_{ij}(\lambda)|^2 = 0 \quad (6)$$

$\gamma^2(\lambda)$ vanishes identically so that (5) no longer applies and the next Taylor term becomes necessary [24]. The next expansion term is quadratic in the parameter vector and corresponds to one half of DTF's Hessian at the point of interest with an $O(n_s^{-1})$ dependence.

The resulting distribution is that of a sum of at most two properly weighted independent χ_1^2 variables where the weights depend on frequency. Explicit computation is left to the Appendix given the need of specialized notation, but can be summarized as

$$n_s (\mathbf{h}_i^H(\lambda) \mathbf{S} \mathbf{h}_i(\lambda)) (|\hat{\gamma}_{ij}(\lambda)|^2 - |\gamma_{ij}(\lambda)|^2) \xrightarrow{d} \sum_{k=1}^q l_k(\lambda) \chi_1^2 \quad (7)$$

where $l_k(\lambda)$ are at most two frequency dependent eigenvalues ($q \leq 2$) coming from a matrix that depends on DTF's values. Note that implicit dependence

also comes from the left side of (7) on DTF's denominator. See further details in Proposition 2. Brief comments and explicit computational methods relating sums of χ_1^2 variables may be found in [20], [14] and [25].

These results closely parallel PDC ones in [3], the main difference lying in how the frequency dependent covariance of the parameter vectors are computed.

4 Numerical Illustrations

In the examples that follow dashed lines indicate threshold values and gray shades stand for point confidence intervals around significant points. Unless stated otherwise, innovations noise is zero mean, unit variance and mutually uncorrelated. The frequency domain graphs are displayed in the standard form of an array where grayed diagonal panels contain the estimated time series power spectra.

Example 1 Consider the connectivity from $x_1 \rightarrow x_2$ whose dynamics is represented by an oscillator which influences another structure without feedback:

$$\begin{aligned} x_1(n) &= 0.95\sqrt{2}x_1(n-1) - 0.9025x_1(n-2) + w_1(n) \\ x_2(n) &= -0.5x_1(n-1) + 0.5x_2(n-1) + w_2(n) \end{aligned} \quad (8)$$

As in all bivariate cases, DTF and PDC coincide numerically, yet because DTF computation requires actual matrix inversion in the general case, its null hypothesis threshold limits are affected by the spectra (top panel in Fig. 1) (the $x_1(n)$ in this case) casting decision doubts at $n_s = 50$ points (mid panel) as opposed to the PDC case (bottom panel).

At $n_s = 500$, DTF is above threshold for $x_1 \rightarrow x_2$ throughout the frequency interval (Fig. 2). Further comparison is provided in Fig. 3a where the actually observed DTF values for $n_s = 50$ are more spread than those in Fig. 3b for $n_s = 500$. In the $x_2 \rightarrow x_1$ direction, (7) behaviour is readily confirmed.

Even though bivariate DTF and PDC numerically coincide, the need to take into account $\bar{\mathbf{A}}(\lambda)$ inversion under the DTF's null hypothesis can lead to overly conservative thresholds and consequent failure to properly reject H_0 if n_s is small as in Fig. 1.

Example 2 This example shows an oscillator $x_1(n)$ whose influence travels back to itself through a loop containing the $x_2(n) \rightarrow x_3(n)$ link in the feedback loop pathway (Fig. 4) and whose dynamics follows:

$$\begin{aligned} x_1(n) &= 0.95\sqrt{2}x_1(n-1) - 0.9025x_1(n-2) \\ &\quad + 0.35x_3(n-1) + w_1(n) \\ x_2(n) &= 0.5x_1(n-1) + 0.5x_2(n-1) + w_2(n) \\ x_3(n) &= x_2(n-1) - 0.5x_3(n-1) + w_3(n) \end{aligned} \quad (9)$$

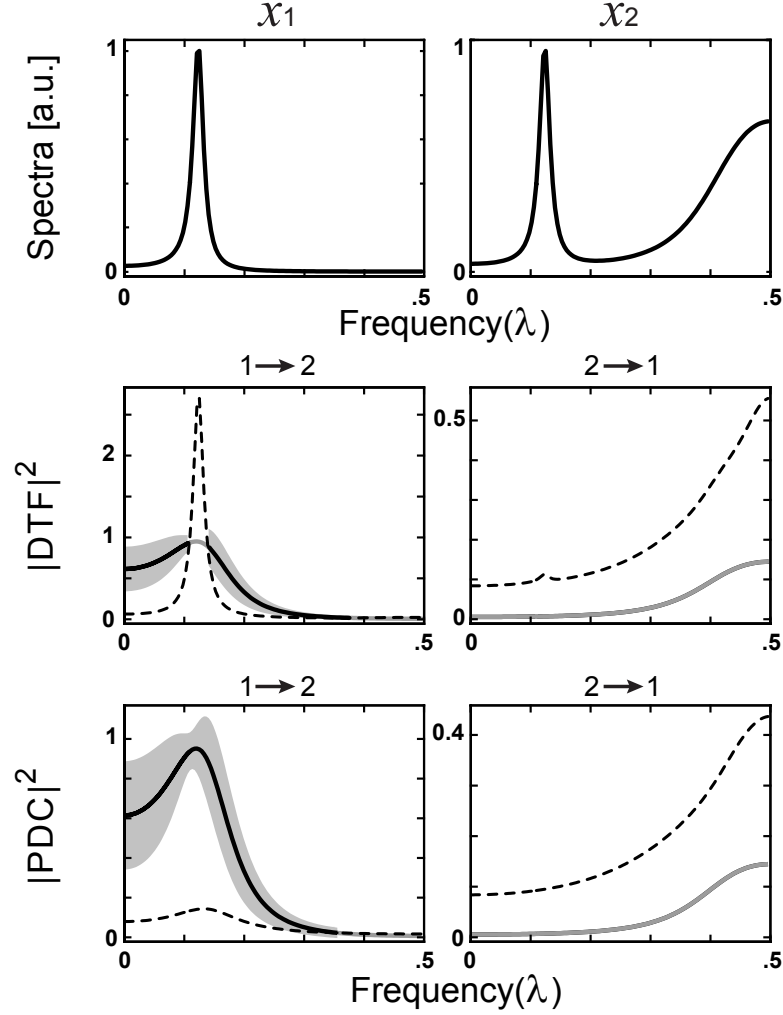


Figure 1: Comparison between DTF (middle row) and PDC (bottom row) for Ex. 1 showing the effect of the existing resonance (time series spectra top row) on threshold decision levels (dashed curves) using $n_s = 50$ simulated data points. The effect of increasing n_s can be appreciated in Fig. 2. Gray shades describe 95% confidence levels when above threshold.

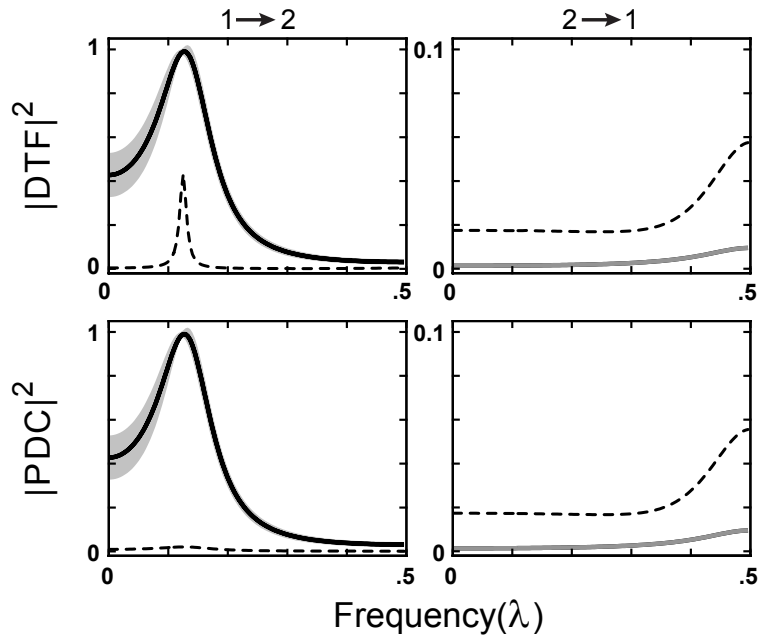


Figure 2: For $n_s = 500$ a DTF single trial realization is safely above threshold - compare it to using $n_s = 50$ in Fig. 1 (middle panel row). Gray shades describe 95% confidence levels when above threshold.

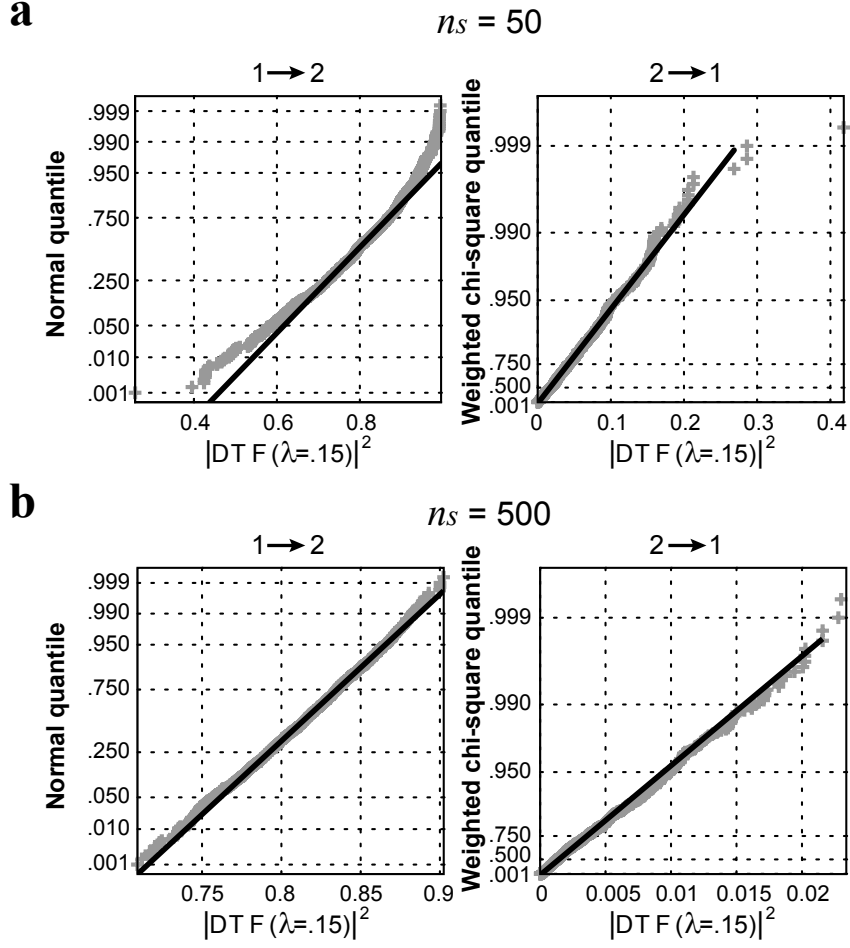


Figure 3: Quantile distribution behaviour showing the distribution goodness of fit improvement as with sample size for Ex. 1 ($n_s = 50$ (a) versus $n_s = 500$ (b)). Statistical spread decrease in the non-existing link $x_2 \rightarrow x_1$ is evident as the improved normal fit of the $x_1 \rightarrow x_2$ existing connection. For each value of n_s , $m = 2000$ simulations were performed.

with the covariance matrix of \mathbf{w} given by

$$\Sigma_{\mathbf{w}} = \begin{bmatrix} 1 & 5 & 0.3 \\ 5 & 100 & 2 \\ 0.3 & 2 & 1 \end{bmatrix}, \quad (10)$$

ensuring that $x_2(n)$ contributes a large amount of innovation power to the loop.

Because ιDTF deals well with unbalanced innovations, it was used with $n_s = 500$ (Fig. 5) and $n_s = 2000$ (Fig. 6) points leading to the following features: (a) the large $|\iota DTF_{i2}|^2$ above 1 for some frequencies are due to the large innovations associated with $x_2(n)$ in (10); (b) except for low ιDTF values that require more points for reliable estimation, calculations confirm that signals originating at any structure reach all other structures; and (c) because of the much smaller relative power originating from $x_3(n)$, its influence is much harder to detect. The allied ιPDC , also shown, confirms which immediate links are directionally active even for $n_s = 500$.

It is interesting to observe that $|\iota DTF_{23}|^2$ has a peak around the x_1 resonance frequency which manifests itself because the innovations originating in x_3 ($w_3(n)$) are filtered by passing through the resonant filter represented by structure x_1 before reaching x_2 . This same type of influence is not so readily apparent (clear only at $n_s = 2000$) in $|\iota DTF_{13}|^2$ because the power contributed by x_3 is small with respect to that of other sources reaching x_1 around that same resonant frequency.

The sharp jump in $|\iota DTF_{32}|^2$ is a byproduct of the fast phase shift that takes place around x_1 's resonance as x_2 's signal travels through it to reach x_3 .

A glimpse of the ensemble ιDTF 's behaviour can be appreciated in Fig. 7 showing how difficult it is to detect it if its values are low.

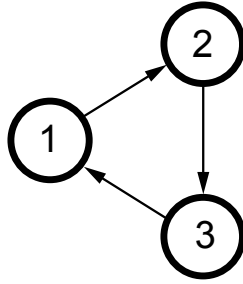


Figure 4: Ex 2 loop connectivity structure. Signals from any structure reach all other structures.

Example 3 The next example comes from [5], whose direct connections are

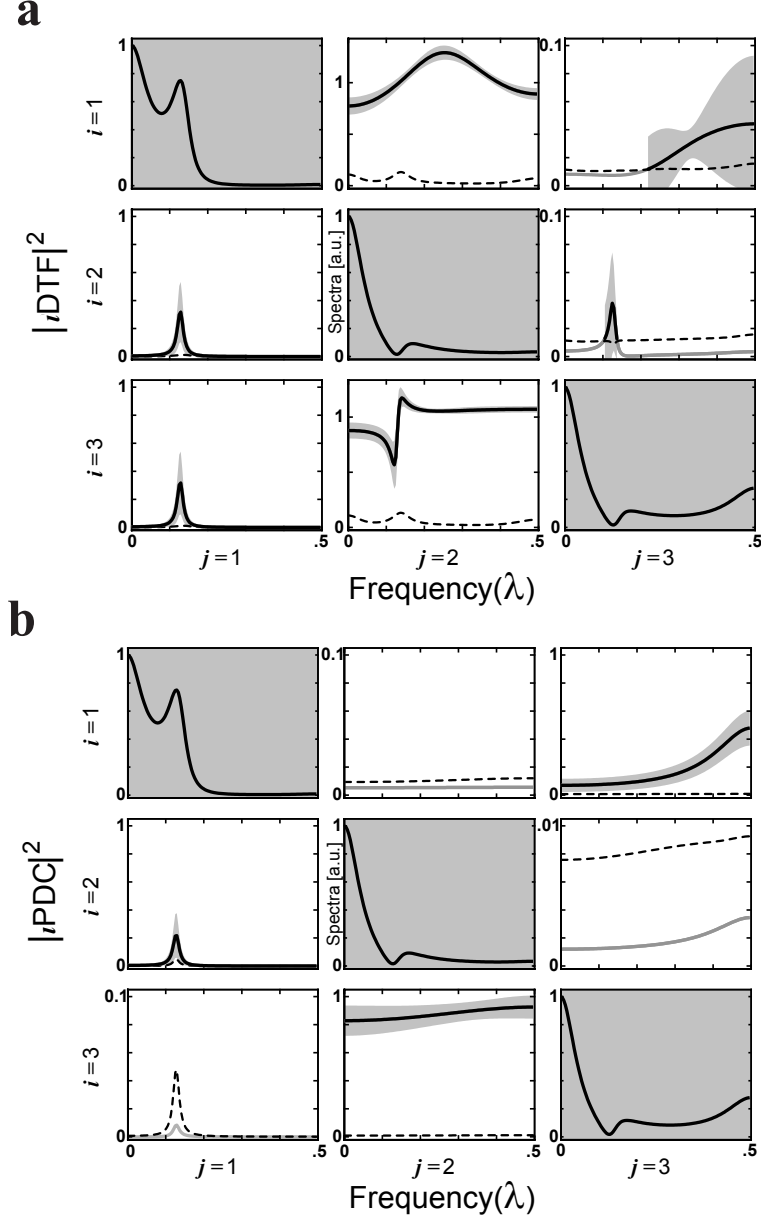


Figure 5: Ex. 2 information ι DTF more widely spread results (**a**) contrasted to ι PDC (**b**) results for $n_s = 500$ and $\alpha = 0.05$. Time series spectra are displayed along the main panel diagonal (gray backgrounds). Sources are marked j (columns) and targets i (rows).

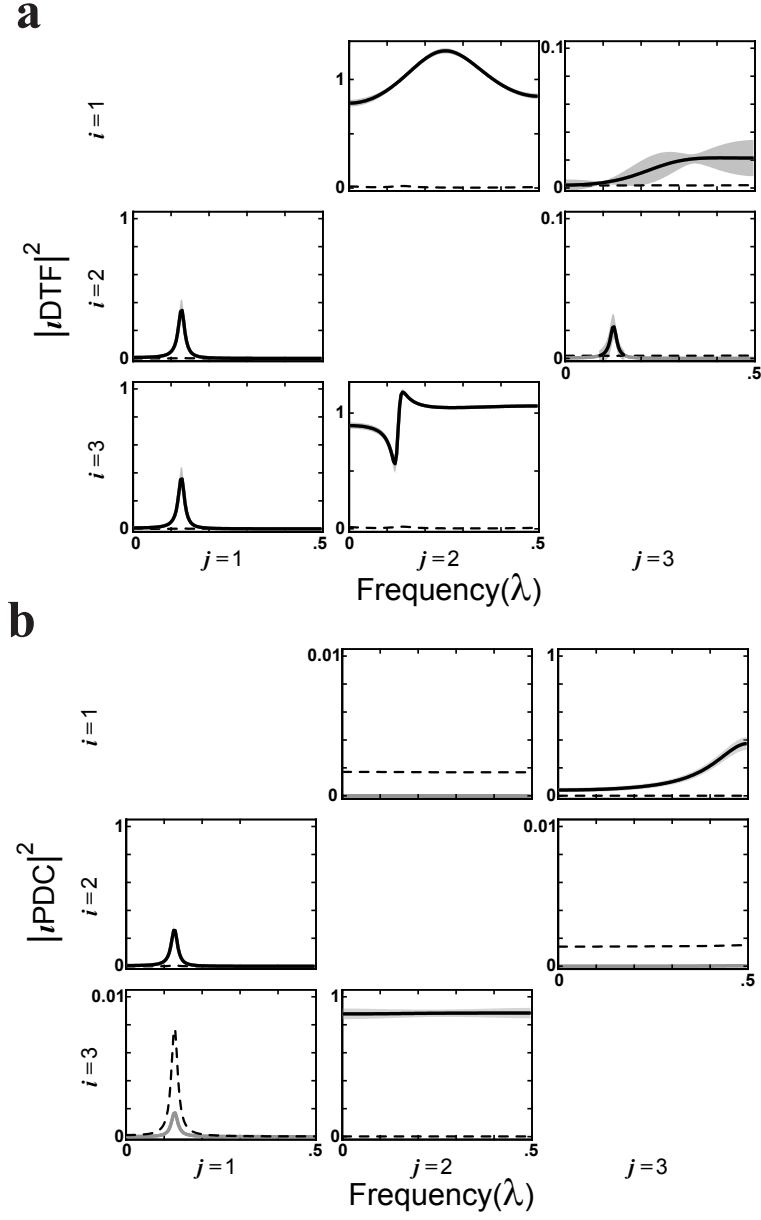


Figure 6: Improvement of connectivity estimates under $n_s = 2000$ over Fig. 5 single trial behaviour using $lDTF$ (a) and $lPDC$ (b). Time series spectra are omitted but can be appreciated from Fig. 5. Sources are marked j and targets i .

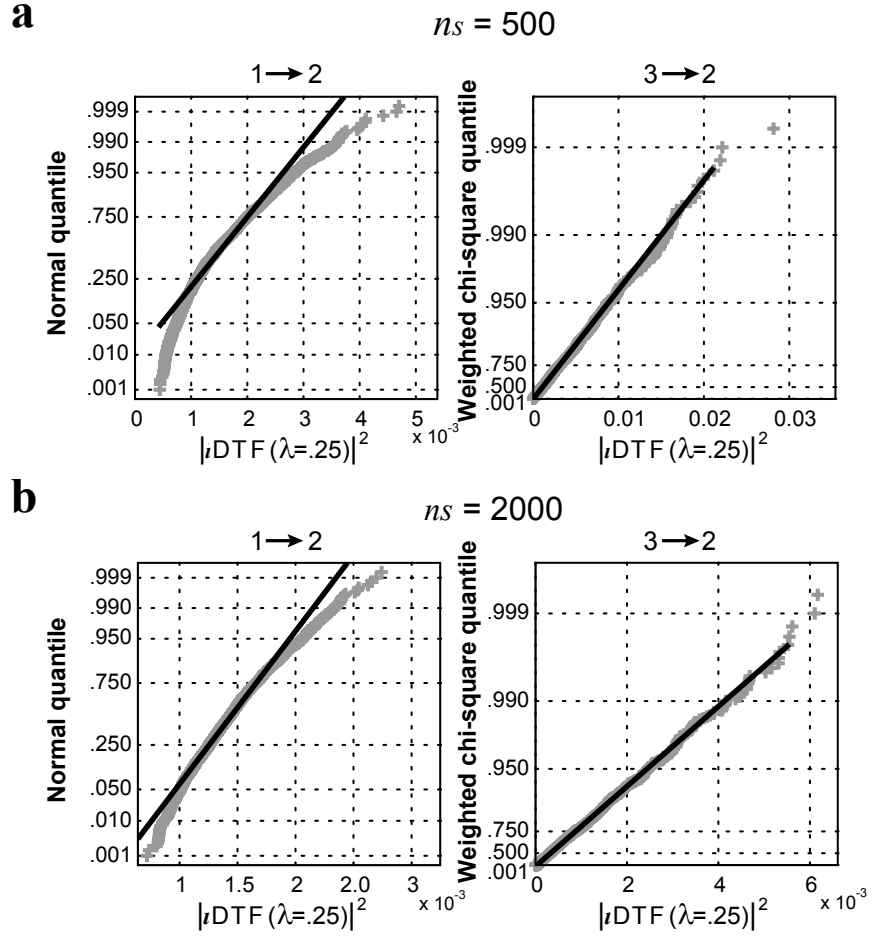


Figure 7: Ex. 2 ι DTF quantile behaviour at $\lambda = 0.25$ for $m = 2000$ simulations using $n_s = 500$ (a) and $n_s = 2000$ (b) data points.

contained in Fig. 8 and are dynamically described by:

$$\begin{aligned}
x_1(n) &= 0.95\sqrt{2}x_1(n-1) - 0.9025x_1(n-2) \\
&\quad + 0.5x_5(n-2) + w_1(n) \\
x_2(n) &= -0.5x_1(n-1) + w_2(n) \\
x_3(n) &= 0.4x_2(n-2) + w_3(n) \\
x_4(n) &= -0.5x_3(n-1) + 0.25\sqrt{2}x_4(n-1) \\
&\quad + 0.25\sqrt{2}x_5(n-1) + w_4(n) \\
x_5(n) &= -0.25\sqrt{2}x_4(n-1) + 0.25\sqrt{2}x_5(n-1) + w_5(n)
\end{aligned} \tag{11}$$

At first sight, signal pathways exist between all structures, i.e. a signal originating at any structure can reach all other structures. Note how difficult it is to pinpoint the x_2 onto x_1 influence even at $n_s = 2000$ (Fig. 9) throughout the frequency domain interval.

The dynamic system (11) was nonetheless designed to have zero influence at some frequencies as can be appreciated by the dip taken by $|\iota DTF_{45}|^2$ whose $x_5 \rightarrow x_4$ influence cannot be detected at its minimum even at $n_s = 2000$ ($\lambda = 0.15$).

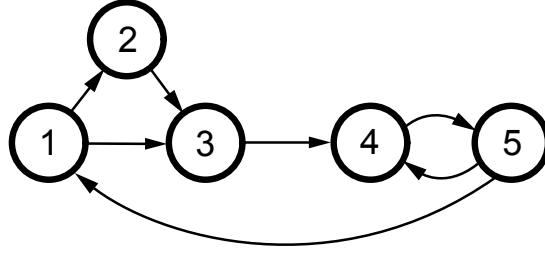


Figure 8: Connectivity diagram for Ex. 3 showing that a signal traveling from any structure can reach any other structure.

Example 4 This last example refers to the connectivity represented in Fig. 10 and behaves dynamically according to

$$\begin{aligned}
x_1(n) &= 0.95\sqrt{2}x_1(n-1) - 0.9025x_1(n-2) \\
&\quad + 0.35x_2(n-1) + w_1(n) \\
x_2(n) &= 0.5x_1(n-1) + 0.5x_2(n-1) + w_2(n) \\
x_3(n) &= x_2(n-1) - 0.5x_3(n-1) + w_3(n)
\end{aligned} \tag{12}$$

whose DTF single trial behaviour can be appreciated in Fig. 11a and b for $n_s = 50$ and $n_s = 500$ respectively, while Fig. 12 sums up its ensemble behaviour between x_1 and x_3 .

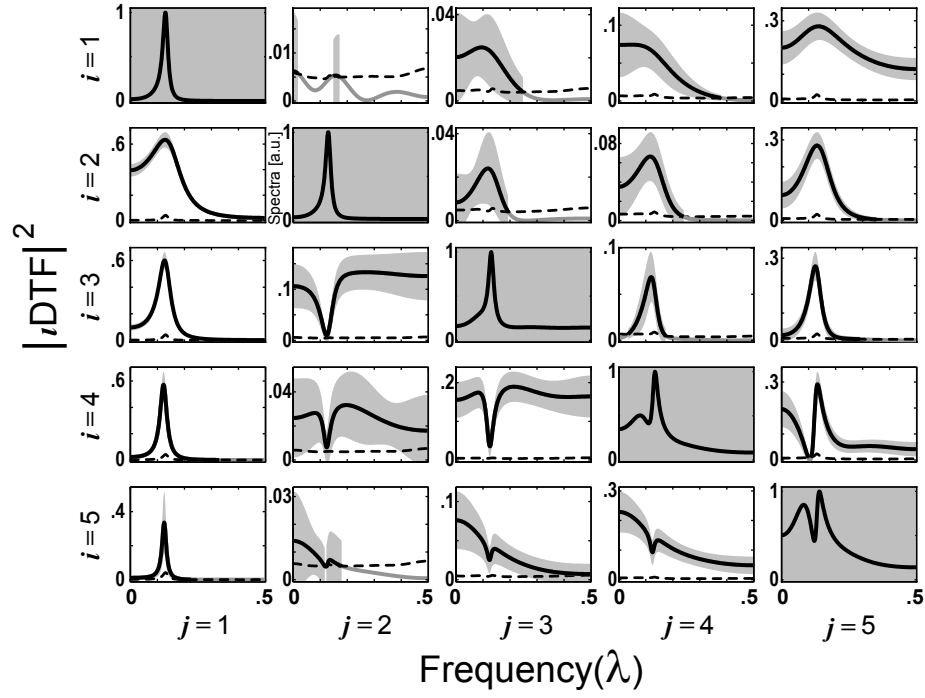


Figure 9: Single trial ι DTF results for the dynamic connectivity ($n_s = 2000$, $\alpha = 0.01$) in Ex. 3. Time series spectra are displayed along the main panel diagonal (gray backgrounds). Note that ι DTF is significant for all pairs (except at some frequencies) confirming that signals from any structures can reach all others. Sources are marked j and targets i .

In this case, there is no x_3 influence on other time series, even though detection is more difficult at $n_s = 50$ (Fig. 11) highlighting the importance of a sufficiently large sample even for such very simple dynamics. This is confirmed by the point quantile distributions in Fig. 12a ($x_1 \rightarrow x_3$) which are somewhat far from the theoretical asymptotic limit, being not yet quite normal compared to the Fig. 12b ($x_1 \rightarrow x_3$) case.

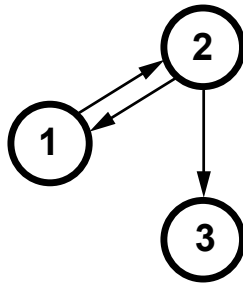


Figure 10: Connectivity diagram between all structures for Ex. 4. Signals from x_3 do not reach the other structures.

5 Discussion

The present unified asymptotics for the DTF forms, introduced respectively in [16], [2] and [27], parallel the recent PDC developments in [3] and [22], confirm early DTF

[16] threshold results [9] and provide estimator confidence intervals and thus pave the way for developing rigorous size effect comparisons using ι DTF and ι PDC under different experimental conditions.

The allied PDCs presented here should not be confused with the purpose of many recent papers [31, 11, 10, 15] that compare connectivity techniques, DTF and PDC among them.

Because many researchers often do not quite realize the conceptual differences between DTF and PDC, this is a good time to stress that they intrinsically measure different aspects of the connectivity between neural structures and neither is conceptually better than the other [15], complementary description aspects emerge when more than just two structures are simultaneously examined. This is clear from Ex. 2 whose loop allows signals from any structures to reach all others - as illustrated by DTF's null hypothesis rejection between all structures at least for some frequencies. By contrast PDC shows the overall direction signals travel within the loop of Ex. 2 by exposing the directional relationship between adjacent structures.

Furthermore, it is also interesting to realize (Ex. 3) that it is entirely possible to have nonzero PDC between pairs of structures and zero DTF between them

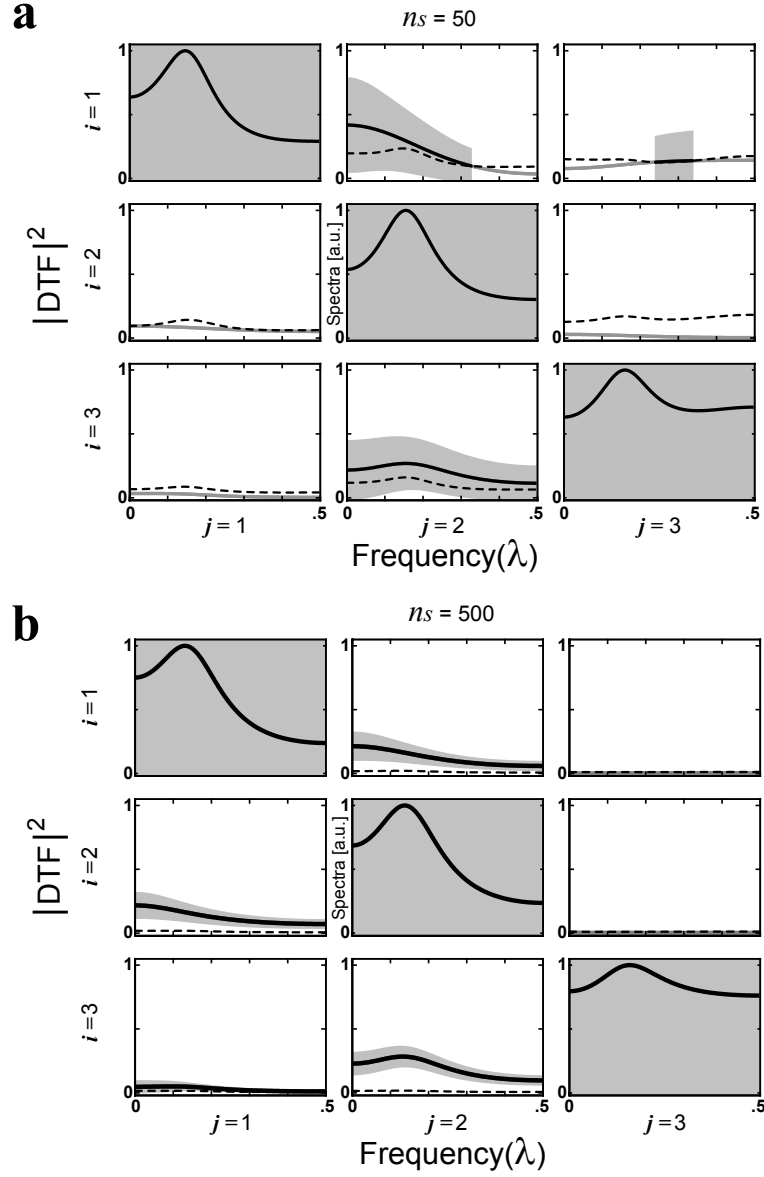


Figure 11: Single trial DTF results for Ex. 4 with $n_s = 50$ (a) and $n_s = 500$ (b), using $\alpha = 0.01$, reflecting the difficulty of inference if n_s is low. Gray shades indicate 99% confidence level for above threshold $|\text{DTF}|^2$.

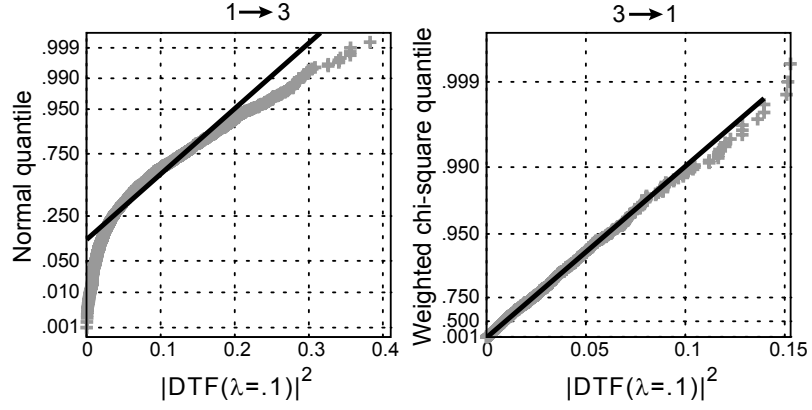
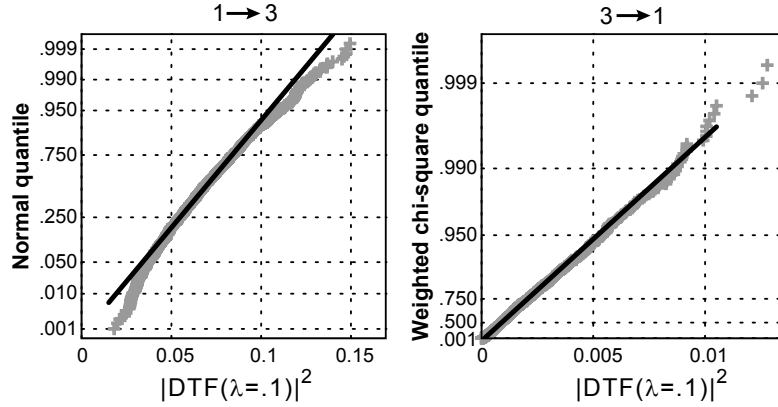
a $n_s = 50$ **b** $n_s = 500$ 

Figure 12: Quantile DTF behaviour for Ex. 4 showing that under $n_s = 50$ the asymptotic normality for the existing link $x_1 \rightarrow x_3$ is not yet reached (**a**) as opposed to (**b**) for $n_s = 500$, using $m = 2000$ simulations in each case. Reasonable fit for the nonexistent reverse connection is observed for both n_s values.

as happens for DTF from x_5 to x_4 in this case in the neighbourhood of the network resonant frequency.

Another DTF contribution as to network description is very well illustrated by the large intrinsic variance of w_2 (x_2 in Ex. 2) ensuring that its influence is comparatively larger upon the other structures; its shape even (see $|\ell\text{DTF}_{32}|^2$ in Fig. 9a) reflects how its originating signal is filtered while traveling through multiple structures. PDC’s descriptive interpretations of the direct immediate link between structures can be further examined in [22].

This newly available objective possibility of performing rigorous hypothesis testing for both DTF and PDC opens up an interesting opportunity in describing neural connectivity. Until now most connectivity has been discussed as either being ‘effective’ and/or ‘functional’, terms coined by [1] and which found widespread employment in functional neuroimaging [12] becoming cornerstone descriptive goals for the recent Connectome effort (see www.connectome.org and [21]).

The popularity of ‘effective’ and ‘functional’ concepts is in line with dynamical network structure descriptions that employ correlation, an undirected quantity that leads to undirected network graphs [29] that stems exactly from the traditional availability of rigorous means for quantifying its statistical reliability even in the light of evidence that its pairwise nature can lead to difficulties in accurate structural description [4].

Furthermore, the effective/functional terminology is confusing: the ‘effective’ term is reserved for situations when dynamical models of some kind are used for network portrayal whereas ‘functional’ usually refers to perceived statistically significant commonalities (correlations) of dynamical behaviour without special reliance on models. The confusion stems from the possibility of functional connectivity even without effective connectivity as when signal pairs covary under the spell of common hidden stimuli and no conceivable anatomical links between them.

Through their complementary vistas on connectivity we have proposed a new “link” centered framework for network connectivity description [7] with PDC describing the immediate direct links between structures and DTF portraying how one structure ultimately influences another. In this new framework, directed links (as opposed to undirected ones as provided by correlation) are the central objects of interest. Links now can be classified according to their state – a directed link is in the *direct-active* state when $\text{PDC} \neq 0$, in the *indirect-active* state if $\text{PDC} = 0$ and $\text{DTF} \neq 0$, is *direct-inactive* for $\text{PDC} = 0$ and *indirect-inactive* when $\text{DTF} = 0$ as proposed in [23] with the present asymptotics for DTF and PDC [3] – affording the necessary operational state identification tools.

Finally, Granger causality (GC), also popular in neural connectivity descriptions, has had conflicting defenses as to whether DTF or PDC, or even other quantities, represent it in the frequency domain. Part of the confusion stems from PDC’s immediate mirror of the Wald type likelihood ratio tests described as GC tests by [19]. Because DTF and PDC indistinguishably reflect GC in the $K = 2$ time series case, but differentiate into distinct network descriptions for $K > 2$, it may worth be developing new terminology to match this dif-

ferentiation. Within the present link centered framework, we propose to split GC into the complementary views of Granger ‘connectivity’ in association with PDC (graph adjacency) and Granger ‘influenciability’ in connection with ‘DTF’ (graph reachability) both now possessing proper rigorous statistical quantification. Our present introduction of G-connectivity to describe immediate structural active connections between structures as opposed to possibly long range influences (G-influenciability) has the intention of standardizing nomenclature and of organizing ideas in our newly proposed paradigm that emphasizes links over structures as the latter must be significantly active in the first place for the meaningful analysis of their interplay to produce neural function.

Appendix

A Propositions

To obtain the results in Sec. 3, specialized notation is needed. The first step is to represent the (3) as vector of real variables by means of the *vec* column stacking operator:

$$\bar{\mathbf{h}}(\lambda) = \text{vec } \mathbf{H}(\lambda) \quad (\text{A.1})$$

and whose associate real vector can be obtained by noting that

$$\mathbf{h}(\lambda) = \begin{bmatrix} \text{Re}(\bar{\mathbf{h}}(\lambda)) \\ \text{Im}(\bar{\mathbf{h}}(\lambda)) \end{bmatrix} = \mathcal{T} \begin{bmatrix} \bar{\mathbf{h}}(\lambda) \\ \bar{\mathbf{h}}^*(\lambda) \end{bmatrix} \quad (\text{A.2})$$

where $*$ denotes complex conjugation and

$$\mathcal{T} = \frac{1}{2} \begin{bmatrix} 1 & 1 \\ -\mathbf{j} & \mathbf{j} \end{bmatrix} \otimes \mathcal{I}_{K^2} \quad (\text{A.3})$$

for $\mathbf{j} = \sqrt{-1}$.

Also let

$$\boldsymbol{\sigma} = \text{vec } \boldsymbol{\Sigma}_{\mathbf{w}}. \quad (\text{A.4})$$

Together (A.1) and (A.4) can be combined in the parameter vector $\boldsymbol{\theta}^T(\lambda) = [\mathbf{h}^T(\lambda) \boldsymbol{\sigma}^T]^T$ so that the problem of computing DTF, in all its forms, can be reduced to that of computing a ratio of quadratic forms

$$|\gamma_{ij}(\lambda)|^2 = \frac{\mathbf{h}^T(\lambda) \mathbf{I}_{ij}^c \boldsymbol{\mathcal{S}}_n(\boldsymbol{\sigma}) \mathbf{I}_{ij}^c \mathbf{h}(\lambda)}{\mathbf{h}^T(\lambda) \mathbf{I}_i^c \boldsymbol{\mathcal{S}}_d(\boldsymbol{\sigma}) \mathbf{I}_i^c \mathbf{h}(\lambda)}, \quad (\text{A.5})$$

by employing the definitions

$$\mathbf{I}_{ij}^c = \begin{bmatrix} \mathbf{I}_{ij} & 0 \\ 0 & \mathbf{I}_{ij} \end{bmatrix} \quad (\text{A.6})$$

and

$$\mathbf{I}_i^c = \begin{bmatrix} \mathbf{I}_i & 0 \\ 0 & \mathbf{I}_i \end{bmatrix}, \quad (\text{A.7})$$

where

1. \mathbf{I}_{ij} whose entries are zero except for indices of the form $(l, m) = ((j-1)K+i, (j-1)K+i)$, which equal 1 whose purpose is to choose the i, j -th element of interest, while
2. \mathbf{I}_i is nonzero only for entries whose indices are of the form $(l, m) : l = m = K(r-1) + i, 1 \leq r \leq K$, and chooses the i -th row of interest from the original (3) matrix,

with $\mathcal{S}_n(\boldsymbol{\sigma})$ and $\mathcal{S}_d(\boldsymbol{\sigma})$ which do not depend on λ and take on different values according to the DTF form under consideration as listed in Table 1.

The proof of (A.5) is immediate and follows of by direct substitution.

A.1 Main Asymptotic Results

The chief basic result is the *delta* method [30] which rests on the continuous mapping nature of the parameters onto the statistics of interest in terms of n_s and the Taylor expansion of the mapping. It is worth summing its content as:

Theorem 1 *If the distribution of $\mathbf{v}_n = (v_1, \dots, v_k)^T$ estimated from n observations converges in distribution as*

$$\sqrt{n}(\mathbf{v}_n - \boldsymbol{\mu}) \xrightarrow{d} \mathcal{N}(0, \boldsymbol{\Sigma}_{\mathbf{v}}). \quad (\text{A.8})$$

Let $g(\mathbf{v})$ be a real-valued function with continuous partials of order $m > 1$ in the neighborhood of $\mathbf{v} = \boldsymbol{\mu}$, with all the partials of order j with $1 \leq j \leq m-1$ vanishing at $\mathbf{v} = \boldsymbol{\mu}$ and non-vanishing m -th order partials at $\mathbf{v} = \boldsymbol{\mu}$. Then

$$\begin{aligned} (\sqrt{n})^m (\hat{g}(\mathbf{v}_n) - g(\boldsymbol{\mu})) &\xrightarrow{d} \frac{1}{m!} \sum_{i_1=1}^k \dots \\ &\sum_{i_m=1}^k \frac{\partial^m g}{\partial x_{i_1} \dots \partial x_{i_m}} \Big|_{x=\boldsymbol{\mu}_{\mathbf{v}}} \prod_{j=1}^m \mathbf{Z}_{i_j}, \end{aligned} \quad (\text{A.9})$$

with

$$\mathbf{Z} = (Z_1, \dots, Z_k)^T \sim \mathcal{N}(0, \boldsymbol{\Sigma}_{\mathbf{v}}), \quad (\text{A.10})$$

wherefrom one can readily deduce the following consequence for large n and non null first derivatives in (A.9):

Corollary 1 *For a real differentiable function $g(\mathbf{v})$ asymptotically distributed as in (A.8) then*

$$\sqrt{n}(\hat{g}(\mathbf{v}_n) - g(\boldsymbol{\mu})) \xrightarrow{d} \mathcal{N}(0, \mathbf{g}^T \boldsymbol{\Sigma}_{\mathbf{v}} \mathbf{g}) \quad (\text{A.11})$$

is the first delta method approximation where $\mathbf{g} = \nabla_{\mathbf{v}} g$ is the gradient of $g(\mathbf{v})$ computed at $\boldsymbol{\mu}$ [24].

Remark 1 Though defined for a scalar function of a vector the results from Corollary 1 remain valid for a vector function where \mathbf{g} then equals the Jacobian of the transformation rather than the gradient see p. 26 Sec. 3.1 in [30].

A.2 Asymptotic θ Behaviour

Proposition 1 The asymptotic properties of θ 's are given by

$$\sqrt{n_s}(\hat{\theta} - \theta) \xrightarrow{d} \mathcal{N}(0, \Omega_\theta) \quad (\text{A.12})$$

where

$$\Omega_\theta = \begin{bmatrix} \Omega_h & \mathbf{0} \\ \mathbf{0} & \Omega_\sigma \end{bmatrix} \quad (\text{A.13})$$

with

$$\Omega_h(\lambda) = \mathcal{H}(\lambda) \mathcal{C}(\lambda) \Omega \mathcal{C}^T(\lambda) \mathcal{H}^T(\lambda) \quad (\text{A.14})$$

for

$$\mathcal{H}(\lambda) = - \begin{bmatrix} \text{Re}(\mathbf{H}^T(\lambda) \otimes \mathbf{H}(\lambda)) & -\text{Im}(\mathbf{H}^T(\lambda) \otimes \mathbf{H}(\lambda)) \\ \text{Im}(\mathbf{H}^T(\lambda) \otimes \mathbf{H}(\lambda)) & \text{Re}(\mathbf{H}^T(\lambda) \otimes \mathbf{H}(\lambda)) \end{bmatrix} \quad (\text{A.15})$$

and

$$\Omega = \begin{bmatrix} \Omega_\alpha & \Omega_\alpha \\ \Omega_\alpha & \Omega_\alpha \end{bmatrix}, \quad (\text{A.16})$$

where Ω_α is the covariance matrix of

$$\alpha = \text{vec}[\mathbf{A}(1) \ \mathbf{A}(2) \ \dots \ \mathbf{A}(p)] \quad (\text{A.17})$$

given by $\Omega_\alpha = \Gamma_{\mathbf{x}}^{-1} \otimes \Sigma_{\mathbf{w}}$, where $\Gamma_{\mathbf{x}} = E[\bar{\mathbf{x}}(n) \bar{\mathbf{x}}^T(n)]$ for

$$\begin{aligned} \bar{\mathbf{x}}(n) &= [x_1(n) \dots x_K(n) \dots \\ &\quad x_1(n-p+1) \dots x_K(n-p+1)]^T; \end{aligned} \quad (\text{A.18})$$

and

$$\Omega_\sigma = 2\mathbf{D}_K \mathbf{D}_K^+ (\Sigma_{\mathbf{w}} \otimes \Sigma_{\mathbf{w}}) \mathbf{D}_K^{+T} \mathbf{D}_K^T \quad (\text{A.19})$$

with \mathbf{D}_K^+ standing for the Moore-Penrose pseudo-inverse of the standard duplication matrix [19] and

$$\mathcal{C}(\lambda) = \begin{bmatrix} \mathbf{C}(\lambda) \\ -\mathbf{S}(\lambda) \end{bmatrix}, \quad (\text{A.20})$$

whose blocks are $K^2 \times pK^2$ dimensional of the form

$$\mathbf{C}(\lambda) = [\mathbf{C}_1(\lambda) \dots \mathbf{C}_p(\lambda)] \quad (\text{A.21})$$

and

$$\mathbf{S}(\lambda) = [\mathbf{S}_1(\lambda) \dots \mathbf{S}_p(\lambda)], \quad (\text{A.22})$$

for

$$\mathbf{C}_r(\lambda) = \text{diag}([\cos(2\pi r\lambda) \dots \cos(2\pi r\lambda)]) \quad (\text{A.23})$$

and

$$\mathbf{S}_r(\lambda) = \text{diag}([\sin(2\pi r\lambda) \dots \sin(2\pi r\lambda)]). \quad (\text{A.24})$$

Table 2: Defining variables according to DTF type in (A.5)

variable	DTF	DC	ι DTF
\mathcal{S}_n	\mathbf{I}_{2K^2}	$\mathbf{I}_2 \otimes (\mathbf{I}_K \odot \boldsymbol{\Sigma}_{\mathbf{w}}) \otimes \mathbf{I}_K$	$\mathbf{I}_2 \otimes (\mathbf{I}_K \odot \boldsymbol{\Sigma}_{\mathbf{w}}) \otimes \mathbf{I}_K$
\mathcal{S}_d	\mathbf{I}_{2K^2}	$\mathbf{I}_2 \otimes (\mathbf{I}_K \odot \boldsymbol{\Sigma}_{\mathbf{w}}) \otimes \mathbf{I}_K$	$\mathbf{I}_2 \otimes \boldsymbol{\Sigma}_{\mathbf{w}} \otimes \mathbf{I}_K$

Proof

The proof follows by noting that $\mathbf{h}(\lambda)$ is a function of $\mathbf{a}(\lambda)$ given by

$$\mathbf{a}(\lambda) = \begin{bmatrix} \text{vec}(\text{Re}(\bar{\mathbf{A}}(\lambda))) \\ \text{vec}(\text{Im}(\bar{\mathbf{A}}(\lambda))) \end{bmatrix} = \begin{bmatrix} \text{vec}(\mathcal{I}_{pK^2}) \\ \mathbf{0} \end{bmatrix} - \mathcal{C}(\lambda)\alpha \quad (\text{A.25})$$

whose covariance matrix is given by (A.16) and is asymptotically independent from $\boldsymbol{\sigma}$ whose covariance is (A.19) as shown in [3].

To obtain $\boldsymbol{\Omega}_{\mathbf{h}}$, first note that the gradient of $\bar{\mathbf{h}}$ in (A.1) can be obtained from

$$\nabla_{\bar{\mathbf{a}}} \bar{\mathbf{h}} = -\mathbf{H}^T \otimes \mathbf{H} \quad (\text{A.26})$$

omitting the explicit λ dependence to simplify notation, in view of (3) in Eq. (1) from See Sec. 10.6, p. 198 in [18].

By writing

$$\begin{bmatrix} \nabla_{\bar{\mathbf{a}}} \bar{\mathbf{h}} \\ \nabla_{\bar{\mathbf{a}}} \bar{\mathbf{h}}^* \end{bmatrix} = \begin{bmatrix} -\mathbf{H}^T \otimes \mathbf{H} & \mathbf{0} \\ \mathbf{0} & -(\mathbf{H}^T \otimes \mathbf{H})^* \end{bmatrix} \begin{bmatrix} \bar{\mathbf{a}} \\ \bar{\mathbf{a}}^* \end{bmatrix} \quad (\text{A.27})$$

and multiplying by \mathcal{T} defined in (A.2) leads to

$$\nabla_{\mathbf{a}} \mathbf{h} = \mathcal{T} \begin{bmatrix} -\mathbf{H}^T \otimes \mathbf{H} & \mathbf{0} \\ \mathbf{0} & -(\mathbf{H}^T \otimes \mathbf{H})^* \end{bmatrix} \mathcal{T}^{-1} = \mathcal{H} \quad (\text{A.28})$$

Therefore the result of Remark 1 implies (A.14) and this completes the proof. \square

A.3 Confidence Interval Theorem

Proposition 2 *Omitting the explicit frequency λ and $\boldsymbol{\sigma}$ dependencies to simplify notation, the confidence interval results*

$$\sqrt{n_s}(|\hat{\gamma}_{ij}|^2 - |\gamma_{ij}|^2) \xrightarrow{d} \mathcal{N}(0, \gamma^2), \quad (\text{A.29})$$

where n_s is the number of observations and

$$\gamma^2 = \mathbf{g}_{\mathbf{h}} \boldsymbol{\Omega}_{\mathbf{h}} \mathbf{g}_{\mathbf{h}}^T + \mathbf{g}_{\boldsymbol{\sigma}} \boldsymbol{\Omega}_{\boldsymbol{\sigma}} \mathbf{g}_{\boldsymbol{\sigma}}^T, \quad (\text{A.30})$$

Table 3: Defining variables according to DTF type in (A.32)

variable	DTF	DC	ι DTF
ξ_n	0	$\text{diag}(\text{vec}(\mathbf{I}_K))$	$\text{diag}(\text{vec}(\mathbf{I}_K))$
ξ_d	0	$\text{diag}(\text{vec}(\mathbf{I}_K))$	\mathbf{I}_{K^2}

for

$$\mathbf{g}_h = 2 \frac{\mathbf{h}^T \mathbf{I}_{ij}^c \mathcal{S}_n \mathbf{I}_{ij}^c}{\mathbf{h}^T \mathbf{I}_i^c \mathcal{S}_d \mathbf{I}_i^c \mathbf{h}} - 2 \frac{\mathbf{h}^T \mathbf{I}_{ij}^c \mathcal{S}_n \mathbf{I}_{ij}^c \mathbf{h}}{(\mathbf{a}^T \mathbf{I}_i^c \mathcal{S}_d \mathbf{I}_i^c \mathbf{h})^2} \mathbf{h}^T \mathbf{I}_i^c \mathcal{S}_d \mathbf{I}_i^c \quad (\text{A.31})$$

and

$$\begin{aligned} \mathbf{g}_\sigma &= \frac{1}{\mathbf{h}^T \mathbf{I}_i^c \mathcal{S}_d \mathbf{I}_i^c \mathbf{h}} [(\mathbf{I}_{ij}^c \mathbf{h})^T \otimes (\mathbf{h}^T \mathbf{I}_{ij}^c)] \boldsymbol{\Theta}_K \xi_n \\ &\quad - \frac{\mathbf{h}^T \mathbf{I}_{ij}^c \mathcal{S}_n \mathbf{I}_{ij}^c \mathbf{h}}{(\mathbf{h}^T \mathbf{I}_i^c \mathcal{S}_d \mathbf{I}_i^c \mathbf{h})^2} [(\mathbf{I}_i^c \mathbf{h})^T \otimes (\mathbf{h}^T \mathbf{I}_i^c)] \boldsymbol{\Theta}_K \xi_d \end{aligned} \quad (\text{A.32})$$

where the values of ξ_n and ξ_d are listed on Table 3 and

$$\begin{aligned} \boldsymbol{\Theta}_K &= (\mathbf{I}_2 \otimes \mathbf{T}_{K^2,2} \otimes \mathbf{I}_{K^2}) \\ &\quad [\text{vec}(\mathbf{I}_2) \otimes (\mathbf{I}_K \otimes \mathbf{T}_{K^2,1} \otimes \mathbf{I}_K)(\mathbf{I}_{K^2} \otimes \text{vec}(\mathbf{I}_K))] \end{aligned} \quad (\text{A.33})$$

with $\mathbf{T}_{L,M}$ standing for the commutation matrix [19].

When the innovation covariance is known *a priori* or does not need to be estimated, the term $\mathbf{g}_\sigma \boldsymbol{\Omega}_\sigma \mathbf{g}_\sigma^T$ in (A.30) is zero.

Proof

This proposition is an immediate consequence of Corollary 1 given the results of Proposition 1 by rewriting (A.5) as

$$\gamma(\boldsymbol{\theta}) = \frac{\gamma_n(\boldsymbol{\theta})}{\gamma_d(\boldsymbol{\theta})} = \frac{\mathbf{h}(\lambda)^T \mathbf{I}_{ij}^c \mathcal{S}_n(\boldsymbol{\sigma}) \mathbf{I}_{ij}^c \mathbf{h}(\lambda)}{\mathbf{h}(\lambda)^T \mathbf{I}_i^c \mathcal{S}_d(\boldsymbol{\sigma}) \mathbf{I}_i^c \mathbf{h}(\lambda)} \quad (\text{A.34})$$

All one needs is to properly compute its gradient or that of its transpose. The job is further simplified by noting the asymptotic independence of \mathbf{h} and $\boldsymbol{\sigma}$ for this allows their separate consideration as $\boldsymbol{\Omega}_\theta$ is block diagonal.

Since DTF is a ratio (see (A.5)) one may write the transpose of the required gradients as

$$\frac{\partial \gamma}{\partial \boldsymbol{\psi}^T} = \frac{1}{\gamma_d^2} \left[\gamma_d \frac{\partial \gamma_n}{\partial \boldsymbol{\psi}^T} - \gamma_n \frac{\partial \gamma_d}{\partial \boldsymbol{\psi}^T} \right] \quad (\text{A.35})$$

where $\boldsymbol{\psi}$ represents either \mathbf{h} or $\boldsymbol{\sigma}$ and respectively leads to \mathbf{g}_h and \mathbf{g}_σ .

Therefore the necessary gradients operate on the required defined quadratic forms whose general differentiation with respect to \mathbf{h} yields

$$\frac{\partial(\mathbf{h}^T \mathbf{I}^c \mathbf{S} \mathbf{I}^c \mathbf{h})}{\partial \mathbf{h}^T} = 2\mathbf{h}^T \mathbf{I}^c \mathbf{S} \mathbf{I}^c \quad (\text{A.36})$$

see p. 175 Eq. (2) in [18]

since all appropriately valued $\mathbf{I}^c \mathbf{S} \mathbf{I}^c$ matrices are symmetric. Inserting the terms in (A.35) leads to (A.31).

The nested dependence of $\gamma(\boldsymbol{\theta})$ on $\boldsymbol{\sigma}$ calls for chain rule use:

$$\frac{\partial(\mathbf{h}^T \mathbf{I}^c \mathbf{S} \mathbf{I}^c \mathbf{h})}{\partial \boldsymbol{\sigma}^T} = \frac{\partial(\mathbf{h}^T \mathbf{I}^c \mathbf{S} \mathbf{I}^c \mathbf{h})}{\partial \mathcal{S}} \frac{\partial \mathcal{S}}{\partial \boldsymbol{\sigma}^T} \quad (\text{A.37})$$

where

$$\frac{\partial(\mathbf{h}^T \mathbf{I}^c \mathbf{S} \mathbf{I}^c \mathbf{h})}{\partial \mathcal{S}} = (\mathbf{I}_{ij}^c \mathbf{h})^T \otimes (\mathbf{h}^T \mathbf{I}_{ij}^c) \quad (\text{A.38})$$

see p. 183 Eq. (3) in [18]

In its general form, $\mathcal{S} = \mathbf{I}_2 \otimes \bar{\mathcal{S}} \otimes \mathbf{I}_K$ (see Table 2). Thus, by the chain rule

$$\frac{\partial \mathcal{S}}{\partial \boldsymbol{\sigma}^T} = \frac{\partial \mathcal{S}}{\partial \bar{\mathcal{S}}} \frac{\partial \bar{\mathcal{S}}}{\partial \boldsymbol{\sigma}^T} \quad (\text{A.39})$$

where

$$\begin{aligned} \frac{\partial \mathcal{S}}{\partial \bar{\mathcal{S}}} &= \boldsymbol{\Theta}_K = (\mathbf{I}_2 \otimes \mathbf{T}_{K^2,2} \otimes \mathbf{I}_{K^2}) \\ &\quad [\text{vec}(\mathbf{I}_2) \otimes (\mathbf{I}_K \otimes \mathbf{T}_{K^2,1} \otimes \mathbf{I}_K)(\mathbf{I}_{K^2} \otimes \text{vec}(\mathbf{I}_K))] \quad (\text{A.40}) \\ &\quad (\text{see p. 184 Eq. (13) in [18]}). \end{aligned}$$

All that is left to compute are the derivatives of $\bar{\mathcal{S}}$ in each case (as in Table 2). For for each possible $\bar{\mathcal{S}}$ value, one has

$$\frac{\partial \mathbf{I}_{K^2}}{\partial \boldsymbol{\sigma}^T} = 0 \quad (\text{A.41})$$

which follows from its lack of $\boldsymbol{\sigma}$ dependence in this case.

When $\bar{\mathcal{S}} = \boldsymbol{\Sigma}_w$,

$$\frac{\partial \boldsymbol{\Sigma}_w}{\partial \boldsymbol{\sigma}^T} = \mathbf{I}_{K^2}. \quad (\text{A.42})$$

Finally considering $\tilde{\mathcal{S}} = \mathbf{I}_K \odot \boldsymbol{\Sigma}_w$ leads to

$$\frac{\partial \tilde{\mathcal{S}}}{\partial \boldsymbol{\sigma}^T} = \text{diag}(\text{vec}(\mathbf{I}_K)) \quad (\text{A.43})$$

see p. 185 eq. (16) in [18].

These results are summarized as $\boldsymbol{\xi}_n$ and $\boldsymbol{\xi}_d$ quantities that appear on Table 3 and comprise (A.32).

The use of Slutsky's lemma concludes the proof by allowing the use of estimated quantities.

□

A.4 Null Hypothesis Test

Under the null hypothesis

$$H_0 : |\gamma_{ij}|^2 = 0 \iff \mathbf{I}_{ij}^c \mathbf{h} = \mathbf{0} \quad (\text{A.44})$$

both (A.31) and (A.32) equal zero, and (5) no longer applies so that the next Taylor term becomes necessary [24] weighted by one half of PDC's Hessian at the point of interest with an $O(n_s^{-1})$ dependence. Via a device similar to that used in [25], one can show that

Proposition 3 *Under (A.44)*

$$n_s(\mathbf{h} \mathbf{I}_i^c \mathcal{S}_d \mathbf{I}_i^c \mathbf{h})(|\hat{\gamma}_{ij}|^2 - |\gamma_{ij}|^2) \xrightarrow{d} \sum_{k=1}^q l_k \chi_1^2 \quad (\text{A.45})$$

where l_k are the eigenvalues of $\mathcal{D} = \mathbf{L}^T \mathbf{I}_{ij}^c \mathcal{S}_n \mathbf{I}_{ij}^c \mathbf{L}$, where \mathbf{L} is the Choleski factor of $\mathbf{\Omega}_{\mathbf{h}}$. Furthermore $q = \text{rank}(\mathcal{D}) \leq 2$, its value is 1 whenever $\lambda \in \{0, \pm 0.5\}$.

The result in (A.45) amounts to a linear combination of χ_1^2 variables whose relative weights depend on estimated parameter and covariance values. Keep in mind that $\mathbf{\Omega}_{\mathbf{h}}$ depends on λ (see eq. (A.14)).

□

Proof

In view of the generalized *delta* method version, Theorem 1 whose conditions call for use of $m = 2$ under H_0 (A.44) since both (A.31) and (A.32) become nullified.

First of all, note that taking derivative of (A.31) and (A.32) with respect to $\boldsymbol{\sigma}$ a second time does not alter the $\mathbf{I}_{ij}^c \mathbf{a}$ dependence and so also produces null results. The same holds when deriving (A.32) with respect to \mathbf{a} since it is quadratic in $\mathbf{I}_{ij}^c \mathbf{a}$.

By contrast, the only nonzero surviving term is that of taking the derivative of (A.31) with respect to \mathbf{a} , which, under H_0 , reduces to

$$\frac{2}{\mathbf{h}^T \mathbf{I}_i^c \mathcal{S}_d \mathbf{I}_i^c \mathbf{h}} \mathbf{I}_{ij}^c \mathcal{S}_n \mathbf{I}_{ij}^c.$$

Therefore the Hessian in (A.9) only has an upper nonzero block corresponding to the derivative of (A.31) with respect to \mathbf{h} so that one only needs to consider the distribution of the latter to write

$$n_s(\hat{\mathbf{h}}^T \mathbf{I}_j^c \mathcal{S}_d \mathbf{I}_j^c \hat{\mathbf{h}})(|\hat{\gamma}_{ij}|^2 - |\gamma_{ij}|^2) \xrightarrow{d} \mathbf{x}^T \mathbf{I}_{ij}^c \mathcal{S}_n \mathbf{I}_{ij}^c \mathbf{x}, \quad (\text{A.46})$$

using Theorem 1 for $\mathbf{x} \xrightarrow{d} \mathcal{N}(0, \mathbf{\Omega}_{\mathbf{h}})$. The use of Slutsky's lemma concludes the first part of the proof by allowing the use of estimated quantities.

Diagonalization of $\mathbf{x}^T \mathbf{I}_{ij}^c \mathcal{S}_n \mathbf{I}_{ij}^c \mathbf{x}$ is done via a transformation through the matrix \mathbf{L} obtained from the Choleski decomposition of $\mathbf{\Omega}_h = \mathbf{L} \mathbf{L}^T$. By making $\mathbf{x} = \mathbf{L} \mathbf{y}$, where $\mathbf{L} = \mathcal{S}_n^{1/2} \mathbf{I}_{ij}^c \mathbf{L}$, yields $\mathbf{x}^T \mathbf{I}_{ij}^c \mathcal{S}_n \mathbf{I}_{ij}^c \mathbf{x} = \mathbf{y}^T \mathbf{L} \mathbf{I}_{ij}^c \mathcal{S}_n \mathbf{I}_{ij}^c \mathbf{L} \mathbf{y} = \mathbf{y}^T \mathbf{D} \mathbf{y}$ so that the elements of the vector $\mathbf{y} = (\mathbf{L}^T \mathbf{L})^{-1} \mathbf{L}^T \mathbf{x}$ are made mutually independent zero mean and of unit variance. Now diagonalizing $\mathbf{D} = \mathbf{U} \mathbf{\Lambda} \mathbf{U}^T$ with $\mathbf{U} \mathbf{U}^T = \mathbf{I}_{q \times q}$ produces

$$\mathbf{y}^T \mathbf{D} \mathbf{y} = \sum_{k=1}^q l_k \mathbf{y}^T \mathbf{u}_k \mathbf{u}_k^T \mathbf{y} = \sum_{k=1}^q l_k \zeta_k^2 \quad (\text{A.47})$$

where \mathbf{u}_k is the k -th column of \mathbf{U} . It is easy to show that the variables $\zeta_k = \mathbf{u}_k^T \mathbf{y}$ are mutually independent, normal zero mean and of unit variance so that ζ_k^2 are χ_1^2 random variables.

As $\text{rank}(\mathbf{X}) = \text{rank}(\mathbf{X}^T)$ and

$$\text{rank}(\mathbf{X} \mathbf{Y}) \leq \min(\text{rank}(\mathbf{X}), \text{rank}(\mathbf{Y})),$$

it follows, after recalling explicit λ dependence, that

$$\begin{aligned} \text{rank}(\mathbf{D}) &= \text{rank}(\mathbf{L}^T \mathbf{I}_{ij}^c \mathcal{S}_n \mathbf{I}_{ij}^c \mathbf{L}) \\ &= \text{rank}(\mathbf{L} \mathbf{L}^T \mathbf{I}_{ij}^c \mathcal{S}_n \mathbf{I}_{ij}^c) \\ &= \text{rank}(\mathbf{\Omega}_h(\lambda) \mathbf{I}_{ij}^c \mathcal{S}_n \mathbf{I}_{ij}^c) \\ &= \text{rank}(\mathcal{H}(\lambda) \mathcal{C}(\lambda) \mathbf{\Omega}_\alpha \mathcal{C}^T(\lambda) \mathcal{H}^T(\lambda) \mathbf{I}_{ij}^c \mathcal{S}_n \mathbf{I}_{ij}^c), \end{aligned} \quad (\text{A.48})$$

which is upper bounded by $\text{rank}(\mathbf{I}_{ij}^c) = 2$. It is readily verified that, when $\lambda \in \{0, \pm 0.5\}$, $\text{rank}(\mathcal{C}(\lambda)) = 1$ imposes the upper bound thus concluding the proof. As for the PDC case [3] if the model order $p = 1$, though a detailed proof is more involved, one can show that the rank of $\mathcal{C}^T(\lambda) \mathcal{H}^T(\lambda) \mathbf{I}_{ij}^c$ equals 1 as it has only a single row that is not identically zero.

□

Acknowledgements

Work done under support from FAPESP (grant 2005/56464-9 – CInAPCe Programme), CAPES Bioinformatics Graduate Programme (D.Y.T.), FAPESP (grant 2008/08171-0 D.Y.T.), Ciência sem Fronteira (D.Y.T.), CNPq (grant 304404/2009-8 L.A.B. and grant 309381/2012 K.S.).

References

- [1] Aertsen AMHJ, Gerstein GL, Habib MK, Palm G (1989) Dynamics of neuronal firing correlation: modulation of “effective connectivity”. *J Neurophysiol*, **61**:900–917

- [2] Baccalá LA, Sameshima K, Ballester G, Valle AC, Timo-Iaria C (1998) Studying the interaction between brain structures via directed coherence and Granger causality. *Appl Signal Process*, **5**:40–48
- [3] Baccalá LA, De Brito CSN, Takahashi DY, Sameshima K (2013) Unified asymptotic theory for all partial directed coherence forms. *Phil Trans R Soc A*, **371**:1–13
- [4] Baccalá LA, Sameshima K (2001a) Overcoming the limitations of correlation analysis for many simultaneously processed neural structures. *Progress in Brain Research, Advances in Neural Population Coding*, **130**:33–47
- [5] Baccalá LA, Sameshima K (2001b) Partial directed coherence: a new concept in neural structure determination. *Biol Cybern*, **84**:463–474
- [6] Baccalá LA, Sameshima K (2014a) Partial directed coherence. In: Sameshima K, Baccalá LA (eds) *Methods in Brain Connectivity Inference through Multivariate Time Series Analysis*. Boca Raton: CRC Press, pp 57–73
- [7] Baccalá LA, Sameshima K (2014b) Multivariate time series brain connectivity: a sum up. In: Sameshima K, Baccalá LA (eds) *Methods in Brain Connectivity Inference through Multivariate Time Series Analysis*. Boca Raton: CRC Press, pp 245–251
- [8] Baccalá LA, Takahashi DY, Sameshima K (2007) Generalized partial directed coherence. In *15th International Conference on Digital Signal Processing*. Cardiff, pp 163–166
- [9] Eichler M (2006) On the evaluation of information flow in multivariate systems by the directed transfer function. *Biol Cybern*, **94**:469–482
- [10] Fasoula A, Attal Y, Schwartz D (2013) Comparative performance evaluation of data-driven causality measures applied to brain networks. *J Neurosci Methods*, **215**:170–189
- [11] Florin E, Gross J, Pfeifer J, Fink GR, Timmermann L (2011) Reliability of multivariate causality measures for neural data. *J Neurosci Methods*, **198**:344–358
- [12] Friston K (1994) Functional and effective connectivity in neuroimaging: a synthesis. *Hum Brain Mapp*, **2**:256–278
- [13] Harary F (1994) *Graph Theory*. Addison-Wesley Series in Mathematics. Boston: Perseus Books
- [14] Imhof JP (1961) Computing the distribution of quadratic forms in normal variables. *Biometrika*, **48**:419–426
- [15] Jovanović A, Perović A, Boročanin M (2013) Brain connectivity measures: computation and comparison. *EPJ Nonlin Biomed Phys*, **1**:1–25

- [16] Kamiński MJ, Blinowska KJ (1991) A new method of the description of the information flow in the brain structures. *Biol Cybern*, **65**:203–210
- [17] Kamiński MJ, Blinowska KJ (2014) Directed transfer function: a pioneering concept in connectivity analysis. In: Sameshima K, Baccalá LA (eds) *Methods in Brain Connectivity Inference through Multivariate Time Series Analysis*. Boca Raton: CRC Press, pp 13–33
- [18] Lütkepohl H (1996) *Handbook of Matrices*. Chichester: John Wiley
- [19] Lütkepohl H (2005) *New Introduction to Multiple Time Series Analysis*. New York: Springer
- [20] Patnaik PB (1949) The non-central χ^2 and F -distributions and their applications. *Biometrika*, **36**:202–232
- [21] Perkel JM (2013) This is your brain: mapping the connectome. *Science*, **339**:350–352
- [22] Sameshima K, Baccalá LA (2014a) Asymptotic PDC properties. In: Sameshima K, Baccalá LA (eds) *Methods in Brain Connectivity Inference through Multivariate Time Series Analysis*. Boca Raton: CRC Press, pp 113–131
- [23] Sameshima K, Baccalá LA (eds) (2014b) *Methods in Brain Connectivity Inference through Multivariate Time Series Analysis*. Boca Raton: CRC Press
- [24] Serfling RJ (1980) *Approximation Theorems of Mathematical Statistics*. New York: Wiley
- [25] Takahashi DY, Baccalá LA, Sameshima K (2007) Connectivity inference between neural structures via partial directed coherence. *J Appl Stat*, **34**:1259–1273
- [26] Takahashi DY, Baccalá LA, Sameshima K (2010a) Frequency domain connectivity: an information theoretic perspective. In *Engineering in Medicine and Biology Society (EMBC), 2010 Annual International Conference of the IEEE*, pp 1726–1729
- [27] Takahashi DY, Baccalá LA, Sameshima K (2010b) Information theoretic interpretation of frequency domain connectivity measures. *Biol Cybern*, **103**:463–469
- [28] Takahashi DY, Baccalá LA, Sameshima K (2014) Information partial directed coherence. In: Sameshima K, Baccalá LA (eds) *Methods in Brain Connectivity Inference through Multivariate Time Series Analysis*. Boca Raton: CRC Press, pp 75–86

- [29] Tononi G, Sporns O, Edelman GM (1994) A measure for brain complexity - relating functional segregation and integration in the nervous system. *Proc Natl Acad Sci USA*, **91**:5033–5037
- [30] van der Vaart AW (1998) *Asymptotic Statistics*. Cambridge: Cambridge University Press
- [31] Vélez-Pérez H, Louis-Dorr V, Ranta R, Dufaut M (2008) Connectivity estimation of three parametric methods on simulated electroencephalogram signals. In *Engineering in Medicine and Biology Society, 2008. EMBS 2008. 30th Annual International Conference of the IEEE*, pp 2606–2609